LETTER Communicated by Eduardo Izquierdo

Active Role of Self-Sustained Neural Activity on Sensory Input Processing: A Minimal Theoretical Model

Bruno A. Santos
bsantos@cefetmg.br
Rogerio M. Gomes
rogerio@cefetmg.br
Federal Center of Technological Education of Minas Gerais, Belo Horizonte, Brazil

Xabier E. Barandiaran
xabier.academic@barandiaran.net
IAS-Research Centre for Life, Mind, and Society, Department of Philosophy, Faculty of Labour Relations and Social Work, University of the Basque Country, 20018 San Sebastián, Spain

Phil Husbands
p.husbands@sussex.ac.uk
Centre for Computational Neuroscience and Robotics. University of Sussex, Falmer, Brighton BM1 9QJ, U.K.

A growing body of work has demonstrated the importance of ongoing oscillatory neural activity in sensory processing and the generation of sensorimotor behaviors. It has been shown, for several different brain areas, that sensory-evoked neural oscillations are generated from the modulation by sensory inputs of inherent self-sustained neural activity (SSA). This letter contributes to that strand of research by introducing a methodology to investigate how much of the sensory-evoked oscillatory activity is generated by SSA and how much is generated by sensory inputs within the context of sensorimotor behavior in a computational model. We develop an abstract model consisting of a network of three Kuramoto oscillators controlling the behavior of a simulated agent performing a categorical perception task. The effects of sensory inputs and SSAs on sensory-evoked oscillations are quantified by the cross product of velocity vectors in the phase space of the network under different conditions (disconnected without input, connected without input, and connected with input). We found that while the agent is carrying out the task, sensory-evoked activity is predominantly generated by SSA (93.10%) with much less influence from sensory inputs (6.90%). Furthermore, the influence of sensory inputs can be reduced by 10.4% (from 6.90% to 6.18%) with a decay in the agent's performance of only 2%. A dynamical analysis shows how sensory-evoked oscillations are generated from a dynamic

Neural Computation **34, 686–715** (2022)
https://doi.org/10.1162/neco_a_01471

coupling between the level of sensitivity of the network and the intensity of the input signals. This work may suggest interesting directions for neurophysiological experiments investigating how self-sustained neural activity influences sensory input processing, and ultimately affects behavior.

1 Introduction

The brain spontaneously oscillates all the time regardless of whether someone is daydreaming or mind-wandering or engaged in some cognitive task (Raichle, 2010; Buzsaki, 2006; Cole et al., 2014; Deco, Jirsa, & McIntosh, 2013; Ferezou & Deneux, 2017; Fox & Raichle, 2007; Sporns, 2010). Different mechanisms have been proposed for the generation of spontaneous neural activity at different spatial scales, from the cellular (Dickinson, 1998; Kusters et al., 2007; Hashemi, Valizadeh, & Azizi, 2012) to the network level (Kriener et al., 2014; Tomov, Pena, Roque, & Zaks, 2016; Bojanek, Zhu, & MacLean, 2020; Borges et al., 2020; Santos, Gomes, & Husbands, 2021). This view of an active nervous system has its roots in the work of Brown (1914) and contrasts with the conception of the nervous system as being primarily reflexive and directly driven by stimulus from the environment, which, as Raichle (2010) pointed out, dates back to Sherrington (1906). Although the stimulus-driven approach has made significant progress in understanding some aspects of brain operation, mainly in the sensory areas, it does not take into consideration the majority of neural dynamics, which are internally generated (Vogels, Rajan, & Abbott, 2005). As early as 1950, armed with data from the most advanced EEG recording and analysis equipment of the day, Grey Walter theorized that inherent self-sustained oscillations had a fundamental functional role in perception (Walter, 1950). Since then, a number of experiments have provided evidence that such oscillatory activity does indeed play a functional, causal role in perceptual tasks and is not noise or incidental background chatter (Romano et al., 2015; Samaha, Iemi, Haegens, & Busch, 2020; Helfrich et al., 2014).

Recent empirical and theoretical research has investigated, from a number of different perspectives, how external stimulation interacts with spontaneous neural oscillations to generate sensory-evoked dynamics underlying behavior (Samaha et al., 2020; Pachitariu, Lyamzin, Sahani, & Lesica, 2015; Romano et al., 2015; Sarracino, Arviv, Shriki, & de Arcangelis, 2020; Belloy et al., 2019; Iemi, Chaumon, Crouzet, & Busch, 2017. Arieli, Sterkin, Grinvald, and Aertsen (1996), for instance, recorded the ongoing and evoked activity in the cat visual cortex and found that evoked responses could be predicted from preceding ongoing activity. They hypothesized that the "ongoing activity must play an important role in cortical function and cannot be ignored in exploration of cognitive processes" (p. 1868). Fisher et al. (2004) analyzed the relationship between spontaneous neural

activity and the response of visual cortical neurons to dynamic scenes and random-noise film images in freely viewing ferrets. They found that sensory-evoked neural activity is generated from the modulation of the ongoing circuit dynamics by input signals rather than simply reflecting the structure of the input signal itself. Cole, Bassett, Power, Braver, and Petersen (2014) used fMRI to measure the temporal relationships between brain regions of subjects performing different tasks. They found that functional networks during task performance are primarily shaped by an intrinsic network present during rest. As they put it, their study establishes a strong relationship between resting-state functional connectivity and task-evoked functional connectivity, areas of neuroscientific inquiry that are typically considered separately. Romano et al. (2015) showed how spontaneous ongoing neural activity in the optic tectum of zebrafish larvae predicted directional tail movements. The spontaneous activity in this brain area, which is central to visually guided behavior, was found to be organized around topographically compact grouping of functionally similar neurons, producing networks that were tuned to behaviorally relevant visual features, thus enabling robust extraction of pertinent sensory information. In a remarkable experiment, Helfrich et al. (2014) were able to manipulate human visual perception by forcing spontaneous brain oscillations of the left and right visual hemispheres into synchrony using externally applied oscillatory stimulation; their findings are strong evidence that it is the neuronal oscillations that drive the visual experience, not the experience driving the oscillations.

Computational models have also been used to investigate a variety of phenomena related to self-oscillating dynamics and sensory input processing (Bick, Panaggio, & Martens, 2018; Moreno & Pacheco, 2004; Strogatz, 2000, 2001). Li, Xue, and Zhang (2020), for example, implemented a fully connected self-oscillating network by using a modified version of the Kuramoto oscillator (Kuramoto, 1975, 2012). They analyzed the collective response of the network to input signals. They found that sensory input stimulates collective synchronized states locked to similar frequencies, associated with a memory mechanism. Another prominent model is the HKB-model, which describes the relative phase dynamic between two nonlinearly coupled oscillators and has the input as a control parameter that changes the vector field from multistable to monostable and eventually metastable (Haken, Kelso, & Bunz, 1985; Kelso, 2009). Santos, Barandiaran, Husbands, Aguilera, and Bedia (2012) and Aguilera, Bedia, Santos, and Barandiaran (2013) used the HKB model to control the behavior of an agent performing sensory gradient climbing behavior. They analyzed the dynamics of the HKB model in a closed sensorimotor loop and found that functional sensory-evoked metastable dynamics are sustained not only by sensory inputs but also by the coordinated coupling of the agent's sensory and motor dynamics.

While these studies demonstrate the fundamental importance of self-sustained oscillatory neural activity (SSA) in sensory processing, many

details remain elusive. The full particulars of how sensory inputs interact with the ongoing spontaneous oscillatory activity are not yet clear, nor are the relative degrees of influence of the sensory input and the inherent oscillations on the resulting sensory-invoked neural signal.The empirical work outlined above emphasizes the complexity of the interaction between sensory input, spontaneous SSA, and sensory-induced neuronal responses (Deco et al., 2013), with the modulation of SSA by sensory inputs being an important element. In order to contribute to this area, in this letter we work with a minimal, and therefore analytically tractable, model that allows us to develop a novel analysis of how sensory inputs interact with spontaneous self-sustained oscillations and ultimately generate sensorimotor behaviors.

We implemented a brain-body-environment system where a simulated robot, controlled by a network of self-oscillating Kuramoto oscillators, performs a categorical perception task (Moioli, Vargas, & Husbands, 2012; Beer, 2003). The central aim of this work is to investigate how much of the sensory-evoked oscillatory activity is generated by SSA in the neural controller and how much is generated by sensory inputs, while the agent is engaged in the task. By using the cross product of velocity vectors to compare the trajectories in a particular state space for the network under different conditions (details in section 2.4), we are able to precisely quantify how much of the task-related oscillations are generated by sensory input (the "sensory effect"), and how much by SSA in the neural circuits. In turn this allows us to give a detailed account of a mechanism whereby sensory-evoked neural oscillations are generated from the modulation of neural SSA by sensory inputs. Specifically, we show how a dynamical coupling between the sensory inputs and the level of sensitivity of the network generate (successful) trajectories in the state space underlying the agent's sensorimotor behavior. The sensitivity surface for the system used in this analysis is generated via our novel measure of sensory effect. The computational model and the methodology used in the analysis are described in section 2.

There have been several previous investigations in this general area (Asai et al., 2003; Moioli et al., 2012; Santos, Barandiaran, & Husbands, 2012; Moioli & Husbands, 2013; Lee, Shin, Gross, & Cho, 2018; Zagha, Casale, Sachdev, McGinley, & McCormick, 2013; Shim & Husbands, 2015), but here we introduce a different perspective. To our knowledge, this is the first attempt to precisely quantify the relative contributions of sensory input and SSA to the evoked signals that are driving a sensorimotor behavior. In tandem with a detailed dynamical systems analysis of the agent and its behavior, this enables us to give a thorough account of how the interactions between of sensory input, SSA, and evoked signals, in the context of the whole brain-body-environment system, give rise to robust sensorimotor behavior. We show that even when the sensory signal is degraded by a significant margin, the agent's performance only declines slightly, suggesting that the interaction between sensory input and SSA is tuned to enable robust

extraction of behaviorally pertinent information, as has been observed in biological systems (Romano et al., 2015).

The next section gives detail of the model—the agent, environment, task, and neural architecture—along with an explanation of how a successful instance of an agent was created for analysis and the methods used for the analysis. Section 3 looks in detail at the successful agent chosen for analysis, describing its behavioral and neural dynamics. That sets up the central analysis, given in section 4, which demonstrates the active role of SSA, showing how it interacts with sensory input to generate robust sensorimotor behavior; an analysis of the relative contributions of SSA and sensory input to the evoked neural signal that drives the behavior is presented. The final section provides conclusions.

2 Theoretical Model and Methods

It is important to point out that the computational model implemented here does not aim at empirical accuracy. It reproduces, at a conceptual level of abstraction, a type of neural dynamics that can be used to investigate the influence of spontaneous oscillations on the processing of sensory inputs in embodied sensorimotor behaviors. The model aims to raise and discuss theoretical issues that could help to understand the dynamical aspects of neural sensory-evoked responses, while being computationally and analytically tractable enough to enable detailed study of the nervous system of a simulated agent engaged in a nontrivial sensorimotor task.

2.1 The Agent and the Task. The task implemented here is inspired by the categorical perception task proposed by Beer (2003). It minimally replicates, at a conceptual level of abstraction, a behavioral phenomenon where a subject has to identify the shape of an object by actively scanning it in order to get sensory stimuli, which will eventually lead to a coherent sensation of the object's shape. Specifically, the model consists of an agent moving back and forth along a horizontal line in a two-dimensional environment, reading the (scaled Euclidean) distance from its sensor to an object placed in a fixed position (see Figure 1). In each trial of the experiment, 20 objects (10 triangles and 10 circles) are presented to the agent in a random sequence. Each object is presented for 6 seconds, and the whole trial lasts 120 seconds. The agent should actively scan the object and move either to the right if it is interacting with a circle or to the left if it is interacting with a triangle. Notice that the agent has to keep interacting with the object during the whole trial (without moving far to the left or to the right) in order to detect the shape transition that might happen every 6 seconds. The sensor activation is scaled such that it is 0 when the agent is vertically aligned with the center of the object and increases as the agent moves to either the right or the left; its maximum value is 1 when the agent is not aligned with any part of the

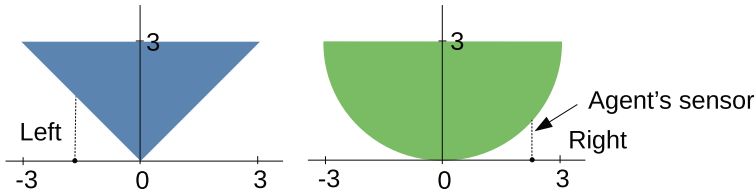

Figure 1: Schematic representation of the simulated environment where the agent is performing the discrimination task. The small black point along the horizontal line represents the agent. Both the base of the triangle and the diameter of the semicircle are 6 units long. The triangle's height and the semicircle's radius are 3 units long. The agent moves along the horizontal line and has a sensor (represented by the dotted line). The sensor returns $d/3$, where d is the Euclidean distance between the agent (dot) and the object's border. The sensor value varies between 0 (agent aligned with the center of the object) and 1 (agent not aligned with any part of the object).

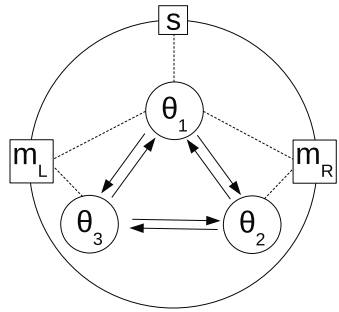

Figure 2: Schematic representation of the agent. The agent has a sensor (s) and two motors (m_L and m_R) and is controlled by a network of three oscillators (θ_1, θ_2, and θ_3).

object. In this way, the sensory input (the sensor reading) varies as the agent moves along the horizontal line.

2.2 The Agent's Controller. The agent is controlled by a network of three phase-coupled oscillators. Only the oscillator θ_1 (described below) is connected to the sensor, which provides continually varying sensory input (s). The agent has two lateral motors, m_R and m_L, where the subscripts R and L stand for right and left (see the schematic representation in Figure 2).

The motor's activations are defined in equations 2.1 and 2.2:

$$m_R = c_1(\cos((\theta_2 - \theta_1) + (2\pi c_2)) + 1), \tag{2.1}$$

$$m_L = c_3(\cos((\theta_3 - \theta_1) + (2\pi c_4)) + 1), \tag{2.2}$$

Table 1: Parameters Evolved by the Genetic Algorithm.

Parameters	Value
$k_{1,2}$	18.387
$k_{1,3}$	1.290
$k_{2,1}$	8.906
$k_{2,3}$	0.417
$k_{3,1}$	0.445
$k_{3,2}$	13.276
w_1	50.67 rad/s
w_2	83.16 rad/s
w_3	101.41 rad/s
c_1	12.613
c_2	0.7873
c_3	18.815
c_4	0.8678
c_5	6.826

where θ_i is the phase of the ith oscillator (explained below) and c_1, c_2, c_3, and c_4 are constant parameters evolved by a genetic algorithm (explained below). The movement of the agent is given by $(m_R - m_L)$, that is, let x denote the centroid of the agent, then $\dot{x} = m_R - m_L$. Each node of the agent's oscillatory network is governed by the Kuramoto's equation defined in equation 2.3 (Kuramoto, 1984):

$$\begin{aligned}
\dot{\theta_1} &= (\omega_1 + s\, c_5) + \sum_{j=1}^{N} k_{j1} sin(\theta_j - \theta_1),\\
\dot{\theta_2} &= \omega_2 + \sum_{j=1}^{N} k_{j2} sin(\theta_j - \theta_2),\\
\dot{\theta_3} &= \omega_3 + \sum_{j=1}^{N} k_{j3} sin(\theta_j - \theta_3),
\end{aligned} \tag{2.3}$$

where θ_i is the phase of the ith oscillator, which is integrated with time step 0.001 seconds using the Euler method, ω_i is a constant representing the ith oscillator's natural frequency, s is the sensory input, c_5 is a constant, N is the number of oscillators (here 3), and k_{ji} is the coupling factor from the jth to the ith oscillator. Note that the sensor s is connected only to the oscillator θ_1. The constant parameters of the model were obtained by a genetic algorithm (explained in section 2.3), and their values are shown in Table 1.

The Kuramoto equation (Kuramoto, 2012) has been used to study a wide range of neural oscillatory phenomena such as the dynamics of cortical

regions and its generative mechanisms (Wilson & Cowan, 1973; Breakspear, Heitmann, & Daffertshofer, 2010), the impacts of topological connectivity in the development of synchronized neural activity (Gómez-Gardeñes, Zamora-López, Moreno, & Arenas, 2010), the effects of lesions on cortical networks oscillations (Honey & Sporns, 2008), and the effects of stimuli on the synchronization dynamics of neurons in the visual cortex (Daza Caro, Tauro, Tamarit, & Gleiser, 2014).

2.3 Methods to Obtain an Agent for the Dynamical Analysis. A synthetic approach (Beer, 1995; Langton, 1997) was taken to produce an agent powered by a phase-coupled network capable of performing the task. A search algorithm was used to find a successful instance of the class of agents described earlier. Such an agent could then be analyzed. The microbial genetic algorithm (Harvey, 2001) was used to adjust the parameters of the model: the motor strengths c_1, c_2, c_3, and c_4; the sensory strength c_5; the natural frequencies $\omega_i \in [50, 110]\text{rad/s}$; and the oscillator connection weights (coupling factors) $k_{i,j} \in [0, 20]$ (numbers in brackets represent the search space bounds for the genetic algorithm). The microbial genetic algorithm is a minimal but effective steady-state GA, in which on each cycle, a member of a geographically distributed (on a 1D torus) population, is randomly selected, followed by another geographically close, randomly selected member; their fitnesses are compared; the winner is replaced back into the population unchanged; and the loser is "infected" with some proportion of the winner's genetic material, via recombination, and then mutated before being put back into the population. Fitter and fitter solutions will evolve as the algorithm proceeds. There is no specific reason why this genetic algorithm was chosen; the system is relatively simple and could have been optimized with other genetic algorithms or search algorithms; the point was to use a search method powerful enough to find successful instances of agents that could then be analyzed to understand their dynamics. The parameters were encoded in a genotype as a vector of real numbers in the range [0,1] and linearly scaled at each trial to their corresponding range. The genetic algorithm setup was population size (30), mutation rate (0.05), recombination (0.60), reflexive mutation, and normal distribution for mutation $(\mu = 0, \sigma^2 = 0.1)$.

In order to subject the agent to the full range of conditions and thus encourage robust behavior (Nolfi, Bongard, Floreano, & Husbands, 2016), each fitness evaluation of an agent consisted of 20 trials. Each trial started at a random initial position within a distance of $[-3, 3]$ units from the center of the object and with a random value of θ_i within $[0, 2\pi)$ radians. A total of 10 circles and 10 triangles were presented to the agent as a random sequence during each trial. Each object was presented for 6.0 seconds, giving a total of 120 seconds for a trial. That is, the shape of the object may or may not change every 6 s, but it is guaranteed the agent will interact with 10 circles and 10 triangles during a trial (120 s). At the end of each trial, the fitness of

the agent was measured by

$$
\begin{aligned}
F_{trial} &= F_{triangle}F_{circle};\\
F_{triangle} &= \frac{1}{10}\sum_{p=1}^{10}\begin{cases}1; & \text{if } d_f < 0;\\ 0; & \text{otherwise};\end{cases}\\
F_{circle} &= \frac{1}{10}\sum_{p=1}^{10}\begin{cases}1; & \text{if } d_f > 0;\\ 0; & \text{otherwise};\end{cases}
\end{aligned}
\tag{2.4}
$$

where F_{trial} is the fitness of the agent at the end of a trial; F_{circle} and $F_{triangle}$ are the mean fitness over 10 presentations of circles and triangles, respectively; and d_f is the final distance from the agent to the center of the object at the end of each 6 s section. The final overall fitness of the agent was given by the mean of F_{trial} over the 20 trials. After evolving the parameters until most of the population were highly fit (with mean of $F_{circle} = 0.93$, $F_{triangle} = 0.93$, and $F_{trial} = 0.86$), we ran each individual of the population for an additional 500 trials (without evolving the parameters) and selected the fittest one for the analysis. In total, this fittest agent interacted with 10,000 objects (500 trials with 20 objects in each trial) and correctly responded to the shape of a circle in 95% of the cases and to the shape of a triangle in 97% of the cases. The parameters evolved by a genetic algorithm, which define this fittest agent, to be used for analysis, are shown in Table 1.

2.4 Methods for Dynamical Analysis. The analysis of the model is based on the phase relations between the oscillators defined as $\phi_{1,2} = \theta_1 - \theta_2$, $\phi_{1,3} = \theta_1 - \theta_3$, and $\phi_{2,3} = \theta_2 - \theta_3$. Although in our model, the state space of phase relations consists of three dimensions $\phi_{1,2}$, $\phi_{1,3}$, and $\phi_{2,3}$, it can be reduced to two as one of them can be obtained from the others. We have chosen to analyze $\phi_{1,2}$ and $\phi_{2,3}$ as their dynamics describe the phase relations of oscillators that become transiently synchronized (shown in section 3.2). The phase relations between θ_1 and θ_3 are less interesting since they are continuously desynchronized.

The dynamics of phase relations is studied by analyzing relevant vector fields of the system, here focusing on the spaces $(\phi_{i,j}, \phi_{j,k})$ and $(\dot{\phi}_{i,j}, \dot{\phi}_{j,k})$, the latter being the time derivatives of the phase differences. An illustration of a single vector $\vec{v}$ built from the components $\dot{\phi}_{i,j} = 0.02$ and $\dot{\phi}_{j,k} = 0.01$ is shown in Figure 3A. If $\dot{\phi}_{i,j} = 0$, then the oscillators i and j are phase synchronized. If the magnitude of $\vec{v}$ (which we call a *velocity vector*) is null, then the whole network is phase synchronized as the phase differences between the oscillators are not changing over time. In this work, the effect of the sensory input on the network's spontaneous dynamics was calculated by performing some operations with velocity vectors $\vec{v}$, as follows.

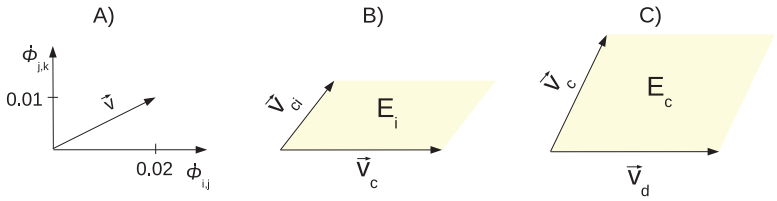

Figure 3: Illustration of the method used to calculate the effect of the sensory input on spontaneous oscillations. (A) A velocity vector obtained from the components $\dot{\phi}_{i,j} = 0.02$ and $\dot{\phi}_{j,k} = 0.01$. (B) Area of the parallelogram obtained from the cross product $\vec{v}_c \times \vec{v}_{ci}$. This area quantifies the effect of the sensory input on the self-sustained oscillations. (C) Area of the parallelogram obtained from the cross product $\vec{v}_d \times \vec{v}_c$. This area quantifies the effect of the interaction between the oscillators and the network dynamics.

For each point in the state space, three velocity vectors were calculated, one for each of the following conditions: (1) a connected network with input ($\vec{v}_{ci}$), (2) a connected network without input ($\vec{v}_c$), and (3) a disconnected network without input ($\vec{v}_d$). When the simulated agent was performing the task, at each time step, $\vec{v}_{ci}$ was calculated by using the current value of sensory input (s), $\vec{v}_c$ was calculated by setting $s = 0$, and $\vec{v}_d$ was calculating by setting $s = 1$ and removing all connections between the oscillators ($k_{j,i} = 0, \forall j, i$). Note that (1) a vector field consisting of vectors $\vec{v}_{ci}$ represents the flow of trajectories of a connected network receiving sensory inputs; (2) a vector field consisting of vectors $\vec{v}_c$ represents the flow of trajectories of a spontaneously oscillating network; and (3) a vector field consisting of vectors $\vec{v}_d$ represents the flow of trajectories of a disconnected network with its components oscillating at their natural frequencies.

The difference between $\vec{v}_{ci}$ and $\vec{v}_c$ quantifies the effect of the sensory input on the spontaneous oscillations. This difference can be measured by the cross product between $\vec{v}_{ci}$ and $\vec{v}_c$, as illustrated in Figure 3B. The magnitude of the resultant vector obtained from the cross product is equal to the area of the parallelogram determined by the two vectors. The greater the area, the greater the difference between $\vec{v}_{ci}$ and $\vec{v}_c$ and also the greater the effect of the sensory input. Formally, the effect of the input can be described as in equation 2.5. It is important to mention that in our model, the modulus of the angle between the vectors is always between 0 and $\frac{\pi}{2}$ as values greater than $\frac{\pi}{2}$ would not correctly represent the effect:

$$E_i = \vec{v}_{ci} \times \vec{v}_c. \tag{2.5}$$

Not only the sensory input but also the connections between the oscillators affect the network dynamics. Following the same rationale, the effect

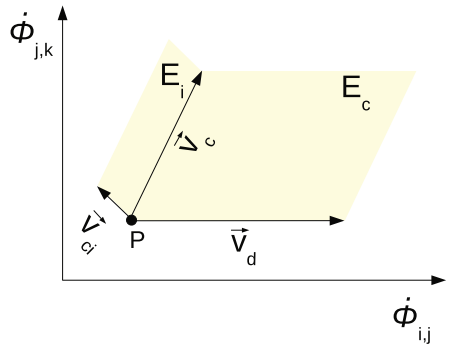

Figure 4: Three vectors ($\vec{v}_d$, $\vec{v}_c$ and $\vec{v}_{ci}$) with origin at P in the state space defined by $\dot{\phi}_{i,j}$ (x-axis) and $\dot{\phi}_{j,k}$ (y-axis). The parallelogram E_c (obtained from $\vec{v}_d \times \vec{v}_c$) depicts the effect of the interactions between the oscillators on the dynamics of a disconnected network. The parallelogram E_i (obtained from $\vec{v}_c \times \vec{v}_{ci}$) represents the effect of sensory inputs on the network self-sustained oscillations.

of the connections can be measured by the cross product between $\vec{v}_c$ and $\vec{v}_d$, as illustrated in Figure 3C. The area of the parallelogram E_c quantifies the effect of the coupling factors on the network operation and can be formally described as in equation 2.6:

$$E_c = \vec{v}_c \times \vec{v}_d. \tag{2.6}$$

The sum of effects from sensory stimulation and the interaction between the oscillators can be written as $E_i + E_c$, as illustrated in Figure 4. Out of the total effect ($E_i + E_c$), the amount due to sensory input can be written as

$$E_{i(R)} = \frac{E_i}{E_i + E_c}. \tag{2.7}$$

$E_{i(R)}$ outputs a value within $[0, 1]$ and represents the relative effect of sensory inputs. If $E_{i(R)} = 1$, the network is driven solely by sensory inputs, and if $E_{i(R)} = 0$, then the network dynamics is driven entirely by its internal activity. Note that each value of $E_{i(R)}$ represents the relative effect at a point of the state space. The total sensory effect considering a set of points (i.e., a trajectory in the state space) can be quantified by summing up the values E_i and E_c at each point and then calculating the total effect as in

$$\varepsilon = \frac{\sum E_i}{\sum E_i + \sum E_c}. \tag{2.8}$$

3 Description of the System Dynamics

This section describes the behavioral and oscillatory network dynamics of the fittest agent evolved for analysis. It provides an initial dynamical analysis of the system that sets up the analysis of the relative effects of sensory input and SSA on the whole embodied sensorimotor behavior which is presented in section 4.

3.1 Agent's Behavior and Its Network Dynamics. This section presents the agent's behavior and the network dynamics during a single trial of the experiment and shows how the network dynamics generates the agent's rightward and leftward movements.

The agent's behavioral response during a single trial of the experiment is presented in Figure 5A. During the first 16 seconds, the agent interacts with a triangle (blue line) continuously moving back and forth along the horizontal line in the range $\approx [-2.5, 0]$. When the object switches to a circle, at $t = 16$ s (green line), the agent goes to the right side of the object and keeps moving back and forth in the range $\approx$[0.7, 2.3]. From $t = 36$ s to $t = 120$ s, the agent correctly responds to a sequence of shape transitions. The time the agent takes to switch sides varies depending on its position and internal state at the moment the shape changes. For instance, while in the time window $t = [42, 48]$ s the agent takes 1.2 s to reach a position where $x > 0$, in the time window $t = [102, 108]$ s it takes 4.4 s (more details about how the agent switches sides are presented in the following).

A zoom into the agent's movement (x), sensor activity (s), and the underlying network dynamics during the interaction with the triangle is shown in Figures 5B1, 5B2, and 5B3, respectively. In this case, the agent converged to a limit cycle (shown in 5B3) with a period of 1.310 s. The agent moves rightward ($\dot{x} > 0$) when its network state is in a dark gray region and leftward ($\dot{x} < 0$) when it is in a light gray region. In the border between these regions, the agent changes the orientation of its movement ($\dot{x} = 0$). At P1 (see Figures 5B1 and 5B3), for instance, the agent changes the orientation of its movement from rightward ($\dot{x} > 0$) to leftward ($\dot{x} < 0$). On the other hand, at P2, the orientation changes from leftward ($\dot{x} < 0$) to rightward ($\dot{x} > 0$). A zoom into the agent's dynamics underlying the interaction with the circle is shown in Figures 5C1, 5C2, and 5C3. In this case, the limit cycle has a shorter period of 0.275 ms. Changes in the agent's orientation are indicated by P3 and P4.

When the network dynamics settles in either limit cycle, the agent keeps oscillating within $x \approx [-2.5, 0]$ for a triangle and within $x \approx [0.7, 2.3]$ for a circle without losing contact with the object (by moving away to the right or the left). The reason for that is that the sum of $\dot{x}$ considering a complete turn around the limit cycle is equal to zero; that is, the sum of movements to the right is equal to the sum of movements to the left. This balance between the sum of negative and positive $\dot{x}$ breaks down when the shape of

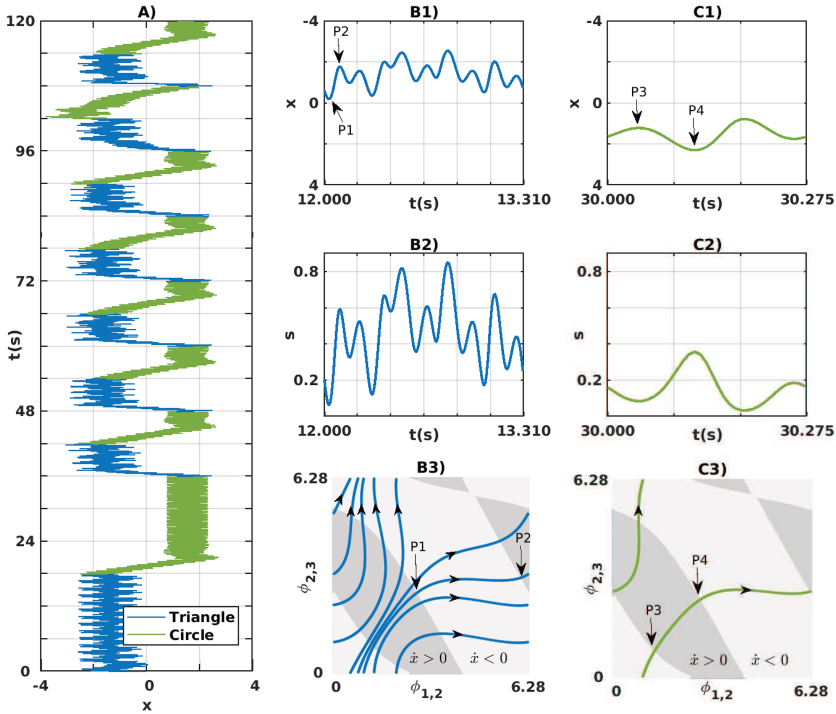

Figure 5: Agent's behavior and its network dynamics during a single trial of the experiment. (A) Agent's position x (x-axis) and time (y-axis). The interaction with a triangle is shown in blue and with a circle in green (see legend). (B1, B2, B3) Zoom ($t = [12, 13.310]$ s) into the agent's movement (x) and sensor activation (s) and network dynamics, respectively, during the interaction with a triangle. Two points P1 and P2 (in panels B1 and B3) highlight two moments where the agent changes the orientation of its movement. The gray color in the background of panel B3 represents the orientation of the agent's movement ($\dot{x} > 0$ for dark gray and $\dot{x} < 0$ for light gray). In the border between these regions, the agent does not move (i.e., $\dot{x} = 0$). (C1, C2, C3) Similar to panels B1 to B3, respectively, but zoom into the interaction with a circle ($t = [30, 30.275]$ s).

the object changes. When the object changes from circle to triangle, for instance, the agent has to move to a position where $x < 0$. This movement is carried out by increasing the sum of negative $\dot{x}$ in relation to the sum of positive $\dot{x}$, as exemplified in Figure 6. From $t = 60.238$ s to $t = 60.430$ s, the agent changes its orientation to leftward and moves from $x = 2.458$ to $x = 0.192$. The network dynamics that generated this leftward movement is represented by the orange trajectory in Figure 6B. Note that this trajectory is passing through a region of $\dot{x} < 0$ (with light gray background). After

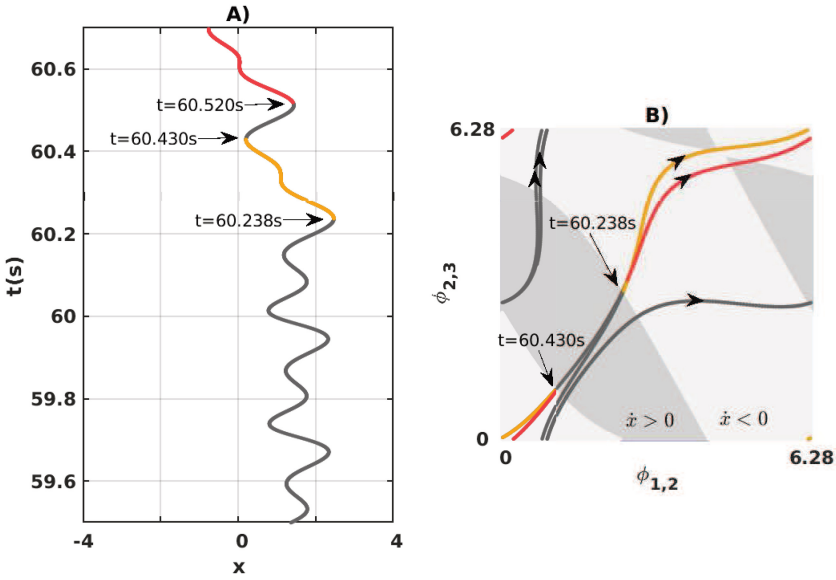

Figure 6: (A) The agent's movement (x-axis) and time (y-axis). At $t = 60$ s, the shape of the object changes from circle to triangle. (B) The network dynamics on the state space. There is correspondence between the colors shown in each graphic: the leftward movement shown in orange in panel A is generated by the orange trajectory shown in panel B.

moving rightward from $t = 60.430$ s to $t = 60.520$ s, the agent again changes its orientation to leftward and moves from $x = 1.428$ to $x = -0.772$, reaching a position where $x < 0$ (see the red line in Figure 6A and the red trajectory in Figure 6B).

This section illustrated the behavior of the agent carrying out a single trial of the experiment, presented two limit cycles to which the network converged, and explained how the dynamics of the network relates to the agent's rightward and leftward movements.

3.2 Natural Frequency and Coupling Factor. In this section, we analyze how the parameters of the network (natural frequencies and coupling factors) contribute to the generation of the network frequency dynamics. The frequency dynamics depends on three variables: (1) natural frequency of the oscillators, (2) coupling factor between oscillators, and (3) effect of the sensory input. When the effect of the sensory input is null, the network converges to self-sustained oscillations, which are generated by combining the natural frequency of the oscillators with their coupling factor. These variables are analyzed throughout this section.

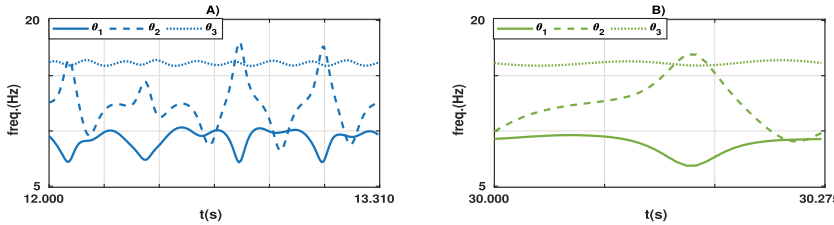

Figure 7: Frequency dynamics of the network corresponding to the agent's behavior presented in Figures 5B1 and 5C1, respectively.

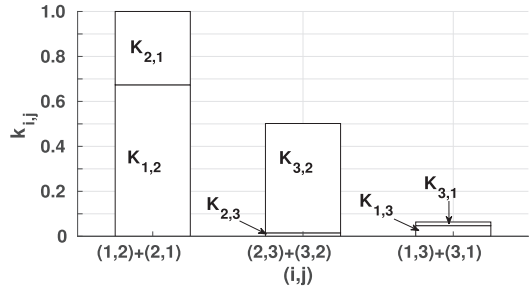

Figure 8: Coupling factor $k_{i,j}$ (y-axis) for each pair of oscillators (i, j) (x-axis) in a scale from 0 to 1.

The frequency dynamics of the network corresponding to the limit cycles shown in Figures 5B3 and 5C3 are presented in Figures 7A and 7B, respectively. The frequency dynamics is characterized by a pattern of alternated synchrony between the pair (θ_1, θ_2) and the pair (θ_2, θ_3). While the oscillators θ_1 and θ_3 do not get synchronized and oscillate at different frequency ranges (around 9 Hz and 16 Hz, respectively), the oscillator θ_2 sometimes synchronizes with θ_1 and sometimes with θ_3.

The natural frequencies of the oscillators are $\omega_1 = 8.06$ Hz (50.67 rad/s), $\omega_2 = 13.23$ Hz (83.16 rad/s), and $\omega_3 = 16.14$ Hz (101.41 rad/s). The values of the coupling factors $k_{i,j}$ are shown in Figure 8. The value of the coupling between θ_1 and θ_2 is the strongest one and between θ_1 and θ_3 the weakest one. The coupling factor between θ_1 and θ_3 is half the value of the coupling between θ_1 and θ_2.

The coupling factor alone does not define the strength of a connection between a pair of oscillators. The strength of a connection depends as well on the difference between the natural frequencies of the oscillators. The same value for the coupling factor $k_{i,j}$ can be considered weak when the difference is relatively high and strong when the difference is relatively low. Table 2 shows the value of the coupling strength in relation to the coupling factor and difference in natural frequencies.

Table 2: Value of the Coupling Strength.

Oscillators	Difference in ω(rad/s)	Coupling Factor	Strength
θ_1 and θ_2	$83.16 - 50.67 = 32.49$	$18.387 + 8.906 = 27.293$	0.840
θ_3 and θ_2	$101.41 - 83.16 = 18.25$	$0.417 + 13.276 = 13.693$	0.750
θ_1 and θ_3	$101.41 - 50.67 = 50.74$	$1.290 + 0.445 = 1.735$	0.034

Notes: First column: pair of oscillators. Second column: difference in natural frequency between the oscillators. Third column: coupling factor. Fourth column: coupling factor divided by the difference in natural frequency.

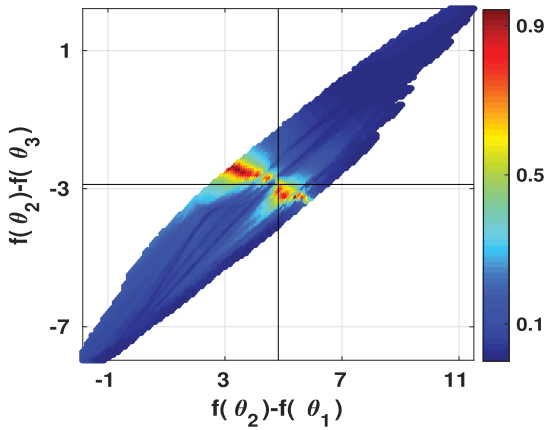

Figure 9: Input effect $E_{i(R)}$ of equation 2.7 (see color bar) in relation to the frequency difference between the oscillators (see axis). The frequency difference $f(\theta_2) - f(\theta_1)$ varies from -1.8 to 11.5 (see x-axis). The frequency difference $f(\theta_2) - f(\theta_3)$ varies from -7.9 to 2.2 (see y-axis). Dashed lines highlight the middle of the frequency differences.

Although the coupling factor $k_{3,2}$ is half the value of $k_{1,2}$ (as shown in Figure 8), the strength of the connection between θ_3 and θ_2 is actually 89% of the strength between θ_1 and θ_2 ($\frac{0.1724}{0.1934} = 0.89$). Note that this result contributes to understanding the two modes of frequency dynamics depicted in Figures 5B3 and 5C3: while the oscillators θ_1 and θ_3 keep oscillating around their natural frequencies, the oscillator θ_2 sometimes synchronizes with θ_1 and sometimes with θ_3.

When θ_2 is synchronized with either θ_1 or θ_3, the sensory input has a low effect on the network activity, as depicted in Figure 9. The highest effect of the sensory input on the frequency dynamics takes place when the network is on the border that divides the regions of frequency synchronization between θ_2 and θ_1 ($f(\theta_2) - f(\theta_1) = 0$ on the x-axis) and between θ_2 and θ_3 ($f(\theta_2) - f(\theta_3) = 0$ on the y-axis), where $f(\theta_i)$ is the frequency of oscillator i.

A more detailed analysis of the relationship between the sensory input effect and the network spontaneous activity is presented in the next section.

4 Active Role of Spontaneous Activity on Sensory Input Processing

The analysis of how spontaneous oscillations actively influence sensory input processing is carried out in two steps. In the first one, presented in section 4.1, we analyze the network dynamics decoupled from the agent's sensorimotor loop. This analysis aims to show how the network's spontaneous activity responds to a "manually" changed input. It sets the ground to understand the process of modulation when the network is coupled to the agent's body constantly receiving sensory inputs, presented in section 4.2.

4.1 Oscillatory Network under Constant Sensory Input. In this section, we analyze the oscillatory network outside the agent's sensorimotor loop by "manually" changing the agent's sensory input (variable s) and studying the effects on the vector field of phase relations.

4.1.1 Modulation of the Vector Field by the Parameter s. The sensory input s modifies the vector field generating different trajectories. Figure 10 shows how s modifies the angle and the magnitude of two example vectors in the state space defined by $\phi_{1,2}$ and $\phi_{2,3}$. The angle and magnitude change differently for each vector (see Figures 10A2, 10A3, 10B2, and 10B3). The magnitude of $\mathbf{v_1}$ decreases from 0.0357 for $s = 0$ to 0.0354 for $s = 1$, and the magnitude of $\mathbf{v_2}$ decreases from 0.0325 for $s = 0$ to 0.0257 for $s = 1$. The angle of $\mathbf{v_1}$ changes from 82.3 degrees for $s = 0$ to 93.4 degrees for $s = 1$ (an increase of 11.1 degrees), and the angle of $\mathbf{v_2}$ changes from 29.3 for $s = 0$ to 35.4 degrees for $s = 1$ (an increase of 6.1 degrees). While $\mathbf{v_1}$ and $\mathbf{v_2}$ change differently, their components $v_{\phi_{1,2}}$ and $v_{\phi_{2,3}}$ undergo the same transformation. The component $v_{\phi_{1,2}}$ linearly decays from 0.0068 between $s = 0$ and $s = 1$ for both $\mathbf{v_1}$ and $\mathbf{v_2}$ (see Figures 10A4 and 10B4), and the component $v_{\phi_{2,3}}$ maintains a constant value for both $\mathbf{v_1}$ and $\mathbf{v_2}$ (see Figures 10A5 and 10B5). The components $v_{\phi_{1,2}}$ and $v_{\phi_{2,3}}$ of all vectors in the vector field undergo the same transformation: $v_{\phi_{1,2}}$ linearly decreases, and $v_{\phi_{2,3}}$ remains constant for all vectors in the vector field; despite that, the transformation in the resultant vector is not linear as it depends on the angle and magnitude of the vector (as exemplified by $\mathbf{v_1}$ and $\mathbf{v_2}$ in Figures 10A1 and 10B1).

4.1.2 Phase Relation Dynamics under Constant Sensory Input. Figure 11 shows the vector fields and the state-space trajectories of phase relations $\phi_{1,2}$ and $\phi_{2,3}$ for $s = 0$, $s = 0.3$, and $s = 1$. The magnitudes of the vectors are greater than zero for $s = 0$, $s = 0.3$, and $s = 1$, showing that θ_1, θ_2, and θ_3 do not all become synchronized together at any time. For $s = 0$, synchronization either takes place between θ_1 and θ_2 or between θ_2 and θ_3 (but not

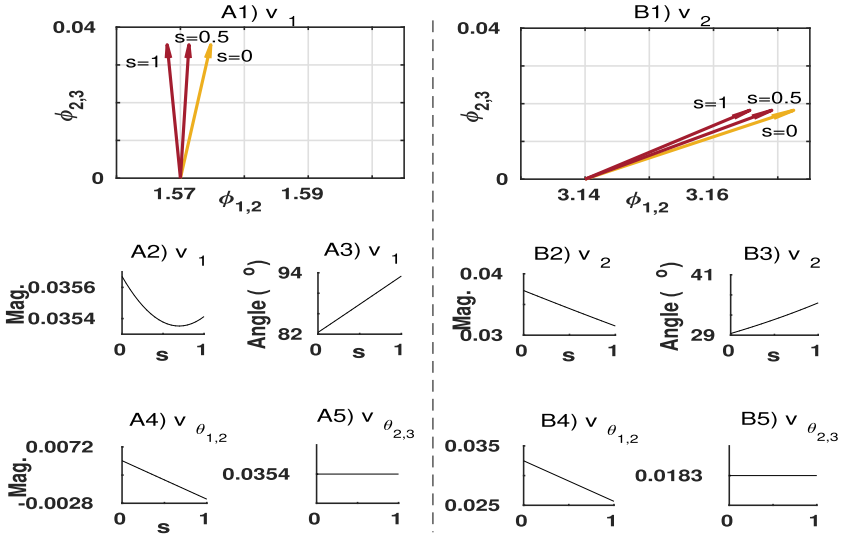

Figure 10: Modulation of two example vectors by the parameter s. The first vector is referred to as $\mathbf{v_1}$, shown in panel A1, at ($\phi_{1,2} = 1.57$, $\phi_{2,3} = 0$). The second vector is referred to as $\mathbf{v_2}$, shown in panel B1, at ($\phi_{1,2} = 3.14$, $\phi_{2,3} = 0$). As the value of the sensory input changes ($s = 0$, $s = 0.5$, and $s = 1$; see the values near the head of each vector), the angle and magnitude of $\mathbf{v_1}$ and $\mathbf{v_2}$ also change. Small graphics underneath show how the angle and magnitude of $\mathbf{v_1}$ and $\mathbf{v_2}$ change for the continuum $s = [0, 1]$ (see panels A2, A3, B2, and B3). The magnitudes of the components for each vector are shown in panels A4 and A5 (for $\mathbf{v_1}$) and panels B4 and B5 (for $\mathbf{v_2}$). See the title of the graphics.

all three); in both cases, the oscillators become synchronized with a phase difference at around 1.57 radians (see the peaks on the density distributions, Figure 11A). For $s = 0.3$, the oscillators do not become synchronized (see the distributions of phase relations in Figure 11B with $H(\phi_{1,2}) = 0.97$ and $H(\phi_{2,3}) = 0.99$, where $H(\phi_{i,j})$ is the Shannon entropy (Shannon, 1948), calculated from the distributions). For $s = 1$, θ_1 and θ_2 are transiently synchronized at around 1.57 radians, and θ_2 and θ_3 are most of the time desynchronized ($H(\phi_{1,2}) = 0.98$). See Figure 11C.

The colored trajectory shown in each graphic depicts the first 300 ms of the phase relation dynamics starting from the same initial state. The main difference between the trajectories can be seen in the range $\phi_{1,2} = [0, 1.57]$ and $\phi_{2,3} = 0$ (bottom left part of the graphics). For $s = 0$ (see Figure 11A), the trajectory turns to the right side (≈ 180 degrees in relation to the x-axis), showing that θ_2 and θ_3 are synchronized and θ_1 and θ_3 desynchronized. For $s = 0.3$ (see Figure 11B), the trajectory follows nearly a diagonal as $\dot{\phi}_{1,2} = \dot{\phi}_{2,3} > 0$ and later turns to the right showing that θ_2 and θ_3 are more

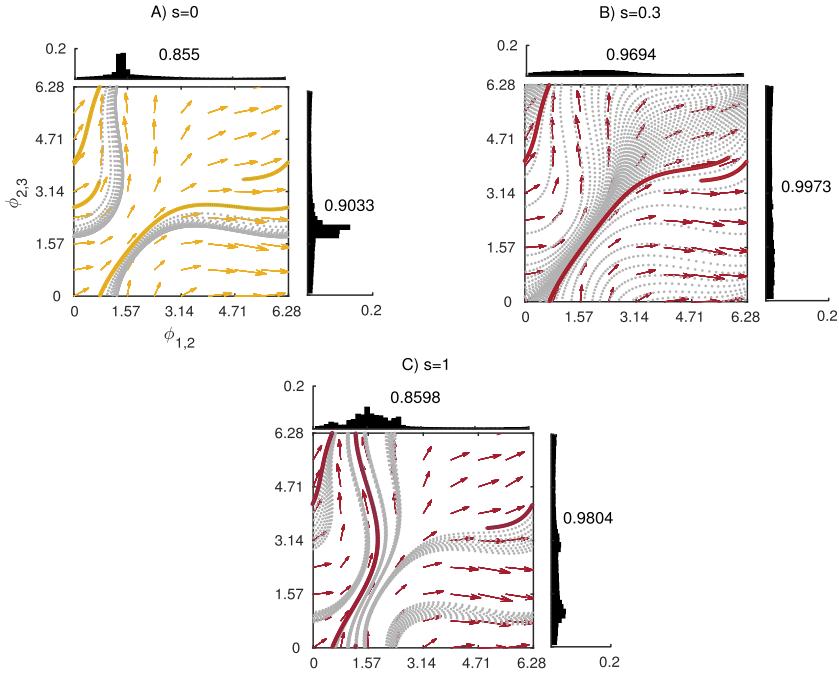

Figure 11: Vector fields and trajectories in the state space of phase relations for $s = 0$ (A), $s = 0.3$ (B), and $s = 1$ (C). The state space is defined by $\phi_{1,2}$ (x-axis) and $\phi_{2,3}$ (y-axis). For ease of visualization, the arrows are three times greater than their original magnitudes. The gray line shows a trajectory in the vector field during a 10 s time window starting at the initial state $\phi_{1,2} = 5.0$ and $\phi_{2,3} = 3.5$ radians. Thick colored lines highlight the first 300 ms of each trajectory. Histograms parallel to the axes show the distribution of phase relations considering the 10 s trajectory. The number near each distribution represents the Shannon entropy.

synchronized than θ_1 and θ_3. For $s = 1$ (see Figure 11C), the trajectory moves upward (≈ 90 degrees in relation to the x-axis), showing that θ_1 and θ_2 are synchronized.

4.1.3 Sensitivity of the Network to Sensory Input. Note that Figures 11A and 11C depict the vector fields of a network without input (s = 0) and maximum input (s = 1), respectively. While trajectories in the vector field shown in Figure 11A correspond to the network's spontaneous oscillations, trajectories in the vector field shown in Figure 11C correspond to the oscillations under the maximum input.

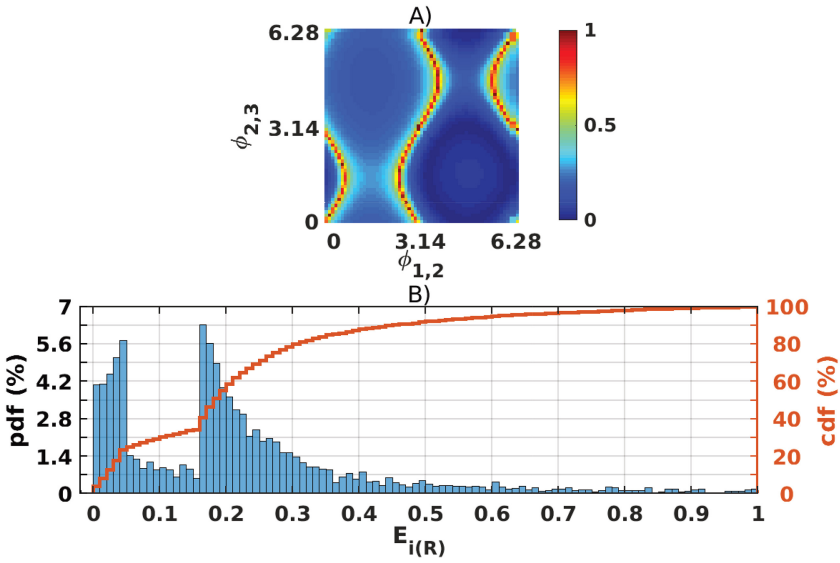

Figure 12: Sensitivity surface of the network to the sensory input. (A) Sensitivity in the state space of phase relations (see axes). (B) Probability density function (pdf) at the left y-axis and cumulative distribution function (cdf) at the right y-axis of the sensitivity (x-axis).

The influence of the sensory input that moves the system from spontaneous to sensory-related oscillations can be measured by $(E_{i(R)})$, as described in equation 2.7. Note that $(E_{i(R)})$ quantifies the difference between two vectors (one generated under s $= 0$ and another under s $\neq 0$) at a specific point of the state space. To obtain the maximum influence that the sensory input can have throughout the state space, the value of s was set to 1, and $(E_{i(R)})$ was calculated for 3600 equally spaced points in the intervals $\phi_{1,2} = [0, 2\pi]$ and $\phi_{2,3} = [0, 2\pi]$. The resulting surface is shown in Figure 12A. This surface is referred to as the sensitivity surface as it defines the maximum effect that an input can have on the network oscillations.

In the dark blue region of the state space, the network dynamics are generated by spontaneous oscillations ($E_{i(R)} \approx 0$). In this region, even high sensory inputs (s $= 1$) have a minor or no effect on the network dynamics. In the light blue region, the network presents low sensitivity to sensory input. Between the light and blue regions, there is a border ($(E_{i(R)} \approx 1)$, represented by red points) where the sensory signals have the highest effect on the network oscillations. The sensitivity is below 0.45 in 90% of the state space (see the cdf of $E_{i(R)}$ on the right y-axis of Figure 12B).

4.1.4 Considerations about the Active Role of Spontaneous Oscillations on Sensory Processing. We observed that the transformation of the resultant vector by the sensory input is not linear, as it depends on the angle and magnitude of the vector (as studied in section 4.1.1 and exemplified by $\mathbf{v_1}$ and $\mathbf{v_2}$ in Figures 10A1 and 10B1). This contributes to understanding why each point of the surface has a different level of sensitivity to sensory input (as studied in section 4.1).

The network's spontaneous dynamics actively participate in sensory processing by establishing different levels of sensitivity to sensory signals. The effect of sensory input on the network operation depends not only on the sensory input itself but also on the level of sensitivity determined by the state of the spontaneously oscillating network. If, for instance, the sensory input is high when the network activity is predominantly generated by internal activity (i.e., low sensitivity) or if the sensory input is low in areas of high sensitivity, then the sensory input will not cause an effect on the oscillatory dynamics.

4.2 Oscillatory Network Coupled to the Sensorimotor Loop.

4.2.1 Dynamic Coupling between Self-Sustained Activity and Sensory Inputs. The section presents how the sensory input dynamics couples to the sensitivity dynamics and generates task-related oscillations.

The values of sensory input, sensitivity, and the relative effect of sensory input under the interaction with circles and triangles are shown in Figure 13. In the limit cycle underlying the interaction with the circle, there are two regions where the network is more open to sensory stimulation (see points P1 and P2 in Figure 13A1). The values of sensitivity at these points are 0.99 and 0.91, respectively. While the sensitivity is high at both points, the input is high only at P1 ($s = 0.36$ at P1 and $s = 0.04$ at P2), as shown in Figure 13A2. As the sensitivity and the input are high at P1, the sensory effect is also high (0.98, shown by P1 in Figure 13A3). On the other hand, a combination of high sensitivity and low input generates a lower sensory effect (0.29) at P2. The sensitivity, the input, and the relative effect of sensory input underlying the interaction with the triangle are shown in Figures 13B1, 13B2, and 13B3, respectively. The two points P1 and P2 with sensitivity equal to 0.50 and 0.97, respectively, are highlighted in Figure 13B1. While at P1, an input of 0.85 generates a sensory effect of 0.46, at P2, a lower input of 0.34 generates a higher sensory effect of 0.90 (values obtained from Figures 13B2 and 13B3).

Note that the intensity of sensory input and the state of the network are dynamically coupled to produce the modulation of the vector field that generates the trajectory corresponding to the task-related oscillations underlying the agent's successful behaviors.

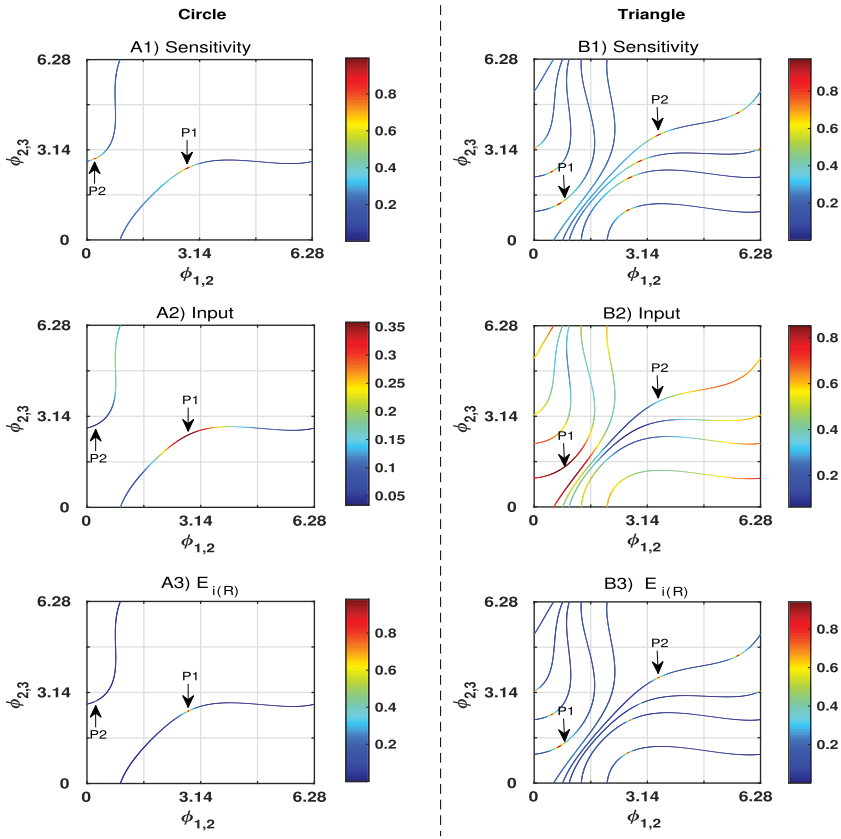

Figure 13: Sensitivity (A1), input (A2), and sensory effect (A3) throughout the limit cycle underlying the interaction with circles. The same graphics for the interaction with triangles are shown in panels B1, B2, and B3. Points P1 and P2 highlight two regions of state space, discussed in the text body.

4.2.2 Effect of the Input on the Network. This section shows how much of the sensory-evoked neural activity is generated by sensory inputs and how much is generated by the network's self-sustained activity.

The distributions of relative sensory effects underlying the interaction with circles and triangles are depicted in Figures 14A and 14B, respectively. For the circle and triangle (see Figures 14A and 14B), 75% of $E_{i(R)}$ values are below 0.05 and 0.17, respectively. During the interaction with both types of objects, 75% of $E_{i(R)}$ values are below 0.13.

While $E_{i(R)}$ represents the relative sensory effect at a point of the state space, the total sensory effect considering a trajectory in the state space can be quantified by ε, as described in equation 2.8. The values of ε for

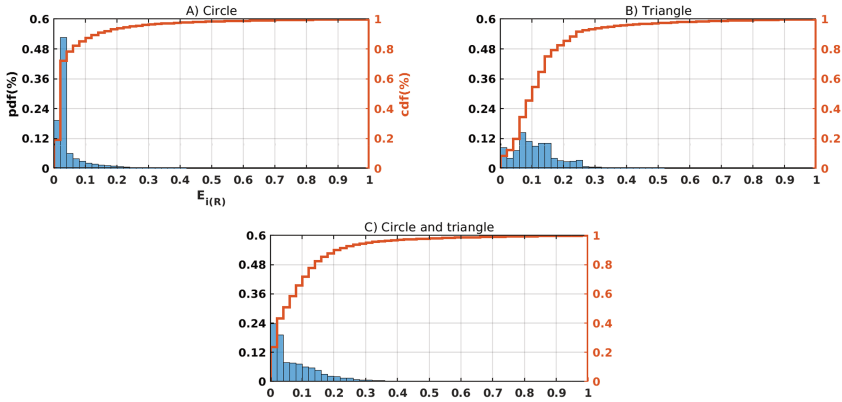

Figure 14: Density distribution for relative sensory effect, $E_{i(R)}$, under interaction with circles (A), triangles (B), and while the agent is carrying out the task, interacting with both types of objects (C). The probability distribution is represented by blue bars with value on the left y-axes. The cumulative distribution is represented by the red line with values on the right y-axes.

Table 3: Sensory Effect on the Network Dynamics.

Interaction	ε
Circle	3.26%
Triangle	9.62%
Circle and triangle	6.90%

Notes: First column: type of object the agent is interacting with. Second column: effect of sensory inputs (in percentage) on the network dynamics.

the network trajectories underlying the interaction with circles, triangles, and both types of objects are shown in Table 3. When the agent is carrying out the task, interacting with circles and triangles, 6.90% of the sensory-evoked neural activity is generated by sensory inputs. When it is interacting only with circles or triangles, the effects are 3.26% and 9.62%, respectively. This analysis shows that most of the sensory-evoked activity is generated by the network's internally generated activity with relatively limited influence from the sensory inputs.

We carried out an additional experiment to find out how much of the total effect (6.90%) is actually exploited by the network to generate the trajectories underlying the agent's successful behavior. To do that, we measured the agent fitness for gradually reduced values of effect ε. The values of ε were reduced by setting a percentage of random sensory inputs to zero

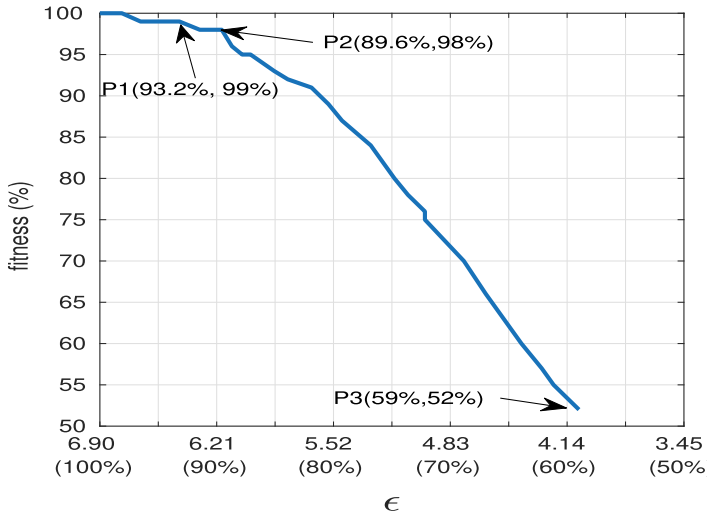

Figure 15: Agent's fitness (y-axis on a scale from 0% to 100%) for different values of effect ε (see inverted x-axis) as sensory input is degraded. Numbers in parentheses on the x-axis show the percentage of ε in relation to its maximum value (6.90). Each value of fitness is the average of 100 trials. See text for further details.

drawn from a uniform distribution over the trial. As shown in Figure 15, the fitness is equal to 99% of the peak fitness (with unreduced ε) for $\varepsilon = 6.43$ (93.2% of original value), which means that if 6.8% (100% − 93.2%) of sensory inputs are discarded, the agent's overall performance is reduced by only 1%. The agent's fitness drops to 98% for $\varepsilon = 6.18$(89.6%), which means that if 10.4% (100% − 89.6%) of sensory inputs are discarded, the agent's behavior degrades by only 2%. From this point onward, the rate of decay increases; for $\varepsilon = 4.07$(59%), for instance, the fitness is equal to 52%; that is, decreasing 41% of the sensory input effect reduces the fitness by 48%.

This finding is reminiscent of the observation that spontaneous neural activity in the visual areas of some animals' brains plays an active role in enabling robust extraction of pertinent sensory information (Romano et al., 2015). In our agent, the interaction between sensory input and SSA is tuned to enable extraction of behaviorally relevant information, even when the sensory signal is degraded, in order to distinguish circles from triangles and complete the required sensorimotor task.

5 Conclusion

Empirical work has posited that sensory-evoked neural oscillations are generated from the modulation of ongoing spontaneous neural dynamics

rather than simply reflecting the structure of the sensory activity itself (Arieli et al., 1996; Fisher et al., 2004; Romano et al., 2015; Samaha et al., 2020). The work described in this letter contributes to the understanding of how this modulation takes place.

The analysis of how the sensory input modulates the vector field of phase relations contributes to explaining why the sensitivity varies throughout the entire state space. It was shown that as the sensory input s increases from 0 to 1, the component $v_{\phi_{1,2}}$ linearly decreases and $v_{\phi_{2,3}}$ maintains a constant value. Despite this linearity, the transformation in the entire vector field is not linear, as it depends on the angle and magnitude of each vector.

We have seen that spontaneous oscillations define different levels of sensory processing sensitivity; these levels were plotted throughout the state space of phase relations and denoted as a sensitivity surface. By defining different levels of sensitivity, the spontaneous oscillations actively participate in sensory input processing. Note that most, if not all, dynamical systems respond differently to sensory inputs depending on their internal states; that is, they have their sensitivity surfaces. What is important in our work is not that the system has a sensitivity surface but how it was built and, consequently, the information it provides us about the operation of the system. The surface was built by quantifying the difference in the trajectories, for each point of the state space, considering the network with (E_i in equation 2.5) and without (E_c in equation 2.6) sensory inputs. From the values of E_i and E_c, the effect of the sensory input in relation to the effect of the self-sustained dynamics was measured on a scale from 0% to 100%, as described in equations 2.7 and 2.8. While equation 2.7 quantified the sensory effect at a specific point of the state space, equation 2.8 quantified the sensory effect for a trajectory in the state space. Although previous work has analyzed the effect of inputs on the spontaneous dynamics of brain-body-environment systems (Fernandez-Leon, 2012; Moioli et al., 2012; Shim & Husbands, 2015), they use different methodologies and consequently give a different perspective on how this interaction takes places.

The points in the sensitivity surface and the trajectories underlying the agent's behavior have shown a predominance of points with a low effect of sensory inputs. When the agent was carrying out the task, interacting with both types of objects, the sensory-evoked activity was predominantly generated by self-sustained activity (93.10%) with relatively little influence from sensory inputs (6.90%). When the sensory influence was reduced by 10.4% (from 6.90% to 6.18%), the agent's performance dropped only by 2%. That is, besides the low influence of sensory inputs on the network trajectories, the network does not depend on the whole set of sensory inputs to sustain the agent's functional behavior.

The analysis of the dynamic coupling between self-sustained activity and sensory inputs showed that task-related oscillatory dynamics underlying the agent's behaviors are not stand-alone entities in a neural system waiting for sensory inputs to be activated. Instead, they are generated by a

fine-grained dynamic coupling between the self-sustained oscillations and the agent's sensory dynamics. The idea of coupled dynamics in brain-body-environment systems is, of course, not new, and has been explored by several researchers (Beer, 2003; Mirolli, 2012; Santos, Barandiaran, Husbands, Aguilera et al., 2012; Aguilera et al., 2013). Those studies have shown, from a variety of perspectives, that the sensory activity dynamically couples to the network's sensitivity-generating trajectories in the state space that will ultimately produce functional sensorimotor coordination. However, to our knowledge, no previous work has systematically quantified the effect of sensory inputs on the network's ongoing dynamics. Here we have quantified how much of the network activity is due to sensory input and how much is due to the agent's internal activity, thus allowing a deeper level of analysis. This quantification was enabled by the novel method described in section 2.4, which has not been used in the context brain-body-environment systems before.

The results obtained from our abstract model may suggest interesting directions for future research that investigates how ongoing neural activity influences sensory input processing and ultimately affects behavior. In this general area, some researchers have tried to predict sensory-evoked neural dynamics based on the ongoing neural activity before the stimulus onset (Barik, Daimi, Jones, Bhattacharya, & Saha, 2019; Samaha et al., 2020; Michail, Toran Jenner, & Keil, 2021). Barik et al. (2019), for instance, predicted, with an accuracy of 75%, the outcome behavior of subjects in a go/no-go task by using the prestimulus ongoing neural activity. Our abstract model can suggest angles to investigate on how these predictions are possible; for example, it is possible that most of the sensory-evoked activity underlying the subject's behavior predominantly consists of prestimulus ongoing dynamics with limited influence from the sensory inputs.

Acknowledgments

X.E.B. acknowledges funding from the Spanish Ministry of Science and Innovation for the research project Outonomy (PID2019-104576GB-I00) and IAS-Research group funding IT 1228-19 from the Basque government.

References

Aguilera, M., Bedia, M. G., Santos, B. A., & Barandiaran, X. E. (2013). The situated HKB model: How sensorimotor spatial coupling can alter oscillatory brain dynamics. *Frontiers in Computational Neuroscience*, *7*, 117. 10.3389/fncom.2013.00117, PubMed: 23986692

Arieli, A., Sterkin, A., Grinvald, A., & Aertsen, A. (1996). Dynamics of ongoing activity: Explanation of the large variability in evoked cortical responses. *Science*, *273*(5283), 1868–1871. 10.1126/science.273.5283.1868, PubMed: 8791593

Asai, Y., Nomura, T., Sato, S., Tamaki, A., Matsuo, Y., Mizukura, I., & Abe, K. (2003). A coupled oscillator model of disordered interlimb coordination in

patients with Parkinson's disease. *Biological Cybernetics*, *88*, 152–162. 10.1007/s00422-002-0371-9, PubMed: 12567229

Barik, K., Daimi, S. N., Jones, R., Bhattacharya, J., & Saha, G. (2019). A machine learning approach to predict perceptual decisions: An insight into face pareidolia. *Brain Informatics*, *6*(1), 1–16. 10.1186/s40708-019-0094-5, PubMed: 30706237

Beer, R. D. (1995). A dynamical systems perspective on agent-environment interaction. *Artificial Intelligence*, *72*, 173–215. 10.1016/0004-3702(94)00005-L

Beer, R. D. (2003). The dynamics of active categorical perception in an evolved model agent. *Adaptive Behavior*, *11*(4), 209–243. 10.1177/1059712303114001

Belloy, M. E., Billings, J., Abbas, A., Kashyap, A., Pan, W.-j., Hinz, R., . . . Keliris, G. A. (2019). *Resting brain fluctuations are intrinsically coupled to visual response dynamics*. bioRxiv:650291.

Bick, C., Panaggio, M. J., & Martens, E. A. (2018). Chaos in Kuramoto oscillator networks. *Chaos: An Interdisciplinary Journal of Nonlinear Science*, *28*(7), 071102. 10.1063/1.5041444

Bojanek, K., Zhu, Y., & MacLean, J. (2020). Cyclic transitions between higher order motifs underlie sustained asynchronous spiking in sparse recurrent networks. *PLOS Computational Biology*, *16*(9), e1007409. 10.1371/journal.pcbi.1007409, PubMed: 32997658

Borges, F., Protachevicz, P., Pena, R., Lameu, E., Higa, G., Kihara, A., . . . Batista, A. (2020). Self-sustained activity of low firing rate in balanced networks. *Physica A: Statistical Mechanics and Its Applications*, *537*, 122671. 10.1016/j.physa.2019.122671

Breakspear, M., Heitmann, S., & Daffertshofer, A. (2010). Generative models of cortical oscillations: Neurobiological implications of the Kuramoto model. *Frontiers in Human Neuroscience*, *4*, 190. 10.3389/fnhum.2010.00190, PubMed: 21151358

Brown, T. G. (1914). On the nature of the fundamental activity of the nervous centres; Together with an analysis of the conditioning of rhythmic activity in progression, and a theory of the evolution of function in the nervous system. *Journal of Physiology*, *48*(1), 18–46. 10.1113/jphysiol.1914.sp001646

Buzsaki, G. (2006). *Rhythms of the brain*. New York: Oxford University Press.

Cole, M. W., Bassett, D. S., Power, J. D., Braver, T. S., & Petersen, S. E. (2014). Intrinsic and task-evoked network architectures of the human brain. *Neuron*, *83*(1), 238–251. 10.1016/j.neuron.2014.05.014, PubMed: 24991964

Daza Caro, Y. C., Tauro, C. B., Tamarit, F. A., & Gleiser, P. M. (2014). Modeling spatial patterns in the visual cortex. *Physical Review E*, *90*(4), 042818.

Deco, G., Jirsa, V. K., & McIntosh, A. R. (2013). Resting brains never rest: Computational insights into potential cognitive architectures. *Trends in Neurosciences*, *36*(5), 268–274. 10.1016/j.tins.2013.03.001, PubMed: 23561718

Dickinson, P. S. (1998). Neuromodulation in invertebrate nervous systems. In M. A. Arbib (Ed.), *The handbook of brain theory and neural networks* (pp. 631–634). Cambridge, MA: MIT Press.

Ferezou, I., & Deneux, T. (2017). How do spontaneous and sensory-evoked activities interact? *Neurophotonics*, *4*(3), 031221–031221. 10.1117/1.NPh.4.3.031221, PubMed: 28630882

Fernandez-Leon, J. A. (2012). Behavioral robustness: An emergent phenomenon by means of distributed mechanisms and neurodynamic determinacy. *Biosystems*, *107*(1), 34–51. 10.1016/j.biosystems.2011.09.002, PubMed: 21963775

Fisher, J., Chiu, C., & Weliky, M. (2004). Small modulation of ongoing cortical dynamics by sensory input during natural vision. *Nature*, *431*(7008), 573.15496914

Fox, M. D., & Raichle, M. E. (2007). Spontaneous fluctuations in brain activity observed with functional magnetic resonance imaging. *Nature Reviews Neuroscience*, *8*(9), 700. 10.1038/nrn2201, PubMed: 17704812

Gómez-Gardeñes, J., Zamora-López, G., Moreno, Y., & Arenas, A. (2010). From modular to centralized organization of synchronization in functional areas of the cat cerebral cortex. *PLOS One*, *5*(8), e12313.

Haken, H., Kelso, J. S., & Bunz, H. (1985). A theoretical model of phase transitions in human hand movements. *Biological Cybernetics*, *51*(5), 347–356. 10.1007/BF00336922, PubMed: 3978150

Harvey, I. (2001). Artificial evolution: A continuing SAGA. In T. Gomi (Ed.), *Lecture Notes in Computer Science: Vol. 2217, Evolutionary robotics: From intelligent robots to artificial life—Proceedings of the of International Symposium on Evolutionary Robotics* (pp. 94–109). Berlin: Springer-Verlag.

Hashemi, M., Valizadeh, A., & Azizi, Y. (2012). Effect of duration of synaptic activity on spike rate of a Hodgkin-Huxley neuron with delayed feedback. *Physical Review E*, *85*(2), 021917. 10.1103/PhysRevE.85.021917

Helfrich, R., Knepper, H., Nolte, G., Struber, D., Rach, S., Hermann, C., . . . Engel, A. K. (2014). Selective modulation of interhemispheric functional connectivity by HD-tACS shapes perception. *PLOS Biology*, *12*, e1002031. 10.1371/journal.pbio.1002031, PubMed: 25549264

Honey, C. J., & Sporns, O. (2008). Dynamical consequences of lesions in cortical networks. *Human Brain Mapping*, *29*(7), 802–809. 10.1002/hbm.20579, PubMed: 18438885

Iemi, L., Chaumon, M., Crouzet, S. M., & Busch, N. A. (2017). Spontaneous neural oscillations bias perception by modulating baseline excitability. *Journal of Neuroscience*, *37*(4), 807–819. 10.1523/JNEUROSCI.1432-16.2016, PubMed: 28123017

Kelso, J. A. (2009). Coordination dynamics. In R. A. Meyers (Ed.), *Encyclopedia of complexity and systems science* (pp. 1537–1565). Berlin: Springer.

Kriener, B., Enger, H., Tetzlaff, T., Plesser, H. E., Gewaltig, M.-O., & Einevoll, G. T. (2014). Dynamics of self-sustained asynchronous-irregular activity in random networks of spiking neurons with strong synapses. *Frontiers in Computational Neuroscience*, *8*, 136. 10.3389/fncom.2014.00136, PubMed: 25400575

Kuramoto, Y. (1975). Self-entrainment of a population of coupled non-linear oscillators. In *Proceedings of the International Symposium on Mathematical Problems in Theoretical Physics* (pp. 420–422). Berlin: Springer.

Kuramoto, Y. (1984). *Chemical oscillations, waves, and turbulence*. New York: Springer.

Kuramoto, Y. (2012). *Chemical oscillations, waves, and turbulence*. New York: Springer Science & Business Media.

Kusters, J., Cortes, J., van Meerwijk, W., Ypey, D., Theuvenet, A., & Gielen, C. (2007). Hysteresis and bistability in a realistic cell model for calcium oscillations and action potential firing. *Physical Review Letters*, *98*(9), 098107. 10.1103/PhysRevLett.98.098107, PubMed: 17359204

Langton, C. (Ed.). (1997). *Artificial life: An overview*. Cambridge, MA: MIT Press.

Lee, B., Shin, D., Gross, S., & Cho, K.-H. (2018). Combined positive and negative feedback allows modulation of neuronal oscillation frequency during sensory processing. *Cell Reports*, *25*, 1548–1560. 10.1016/j.celrep.2018.10.029

Li, X., Xue, T., & Zhang, L. (2020). Information retrieval from modified Kuramoto network by resonant synchronization. *EPL (Europhysics Letters)*, *128*(6), 60002.

Michail, G., Toran Jenner, L., & Keil, J. (2021). Prestimulus alpha power but not phase influences visual discrimination of long-duration visual stimuli. *European Journal of Neuroscience*. 10.1111/ejn.15169

Mirolli, M. (2012). Representations in dynamical embodied agents: Re-analyzing a minimally cognitive model agent. *Cognitive Science*, *36*(5), 870–895. 10.1111/j.1551-6709.2012.01233.x, PubMed: 22417067

Moioli, R. C., & Husbands, P. (2013). Neuronal assembly dynamics in supervised and unsupervised learning scenarios. *Neural Computation*, *25*(11), 2934–2975. 10.1162/NECO_a_00502, PubMed: 23895050

Moioli, R. C., Vargas, P. A., & Husbands, P. (2012). Synchronisation effects on the behavioural performance and information dynamics of a simulated minimally cognitive robotic agent. *Biological Cybernetics*, *106*, 1–21. 10.1007/s00422-012-0507-5, PubMed: 22350535

Moreno, Y., & Pacheco, A. F. (2004). Synchronization of Kuramoto oscillators in scale-free networks. *EPL (Europhysics Letters)*, *68*(4), 603. 10.1209/epl/i2004-10238-x

Nolfi, S., Bongard, J., Floreano, D., & Husbands, P. (2016). Evolutionary robotics. In B. Siciliano & O. Khatib (Eds.), *Springer handbook of robotics* (2nd ed., pp. 2035–2067). Berlin: Springer.

Pachitariu, M., Lyamzin, D. R., Sahani, M., & Lesica, N. A. (2015). State-dependent population coding in primary auditory cortex. *Journal of Neuroscience*, *35*(5), 2058–2073. 10.1523/JNEUROSCI.3318-14.2015, PubMed: 25653363

Raichle, M. E. (2010). Two views of brain function. *Trends in Cognitive Sciences*, *14*(4), 180–190. 10.1016/j.tics.2010.01.008, PubMed: 20206576

Romano, S. A., Pietri, T., Pérez-Schuster, V., Jouary, A., Haudrechy, M., & Sumbre, G. (2015). Spontaneous neuronal network dynamics reveal circuit's functional adaptations for behavior. *Neuron*, *85*(5), 1070–1085. 10.1016/j.neuron.2015.01.027, PubMed: 25704948

Samaha, J., Iemi, L., Haegens, S., & Busch, N. A. (2020). Spontaneous brain oscillations and perceptual decision-making. *Trends in Cognitive Sciences*, *24*, 639–653. 10.1016/j.tics.2020.05.004, PubMed: 32513573

Santos, B. A., Barandiaran, X. E., & Husbands, P. (2012). Synchrony and phase relation dynamics underlying sensorimotor coordination. *Adaptive Behavior*, *20*(5), 321–336. 10.1177/1059712312451859

Santos, B., Barandiaran, X., Husbands, P., Aguilera, M., & Bedia, M. (2012). Sensorimotor coordination and metastability in a situated HKB model. *Connection Science*, *24*(4), 143–161. 10.1080/09540091.2013.770821

Santos, B., Gomes, R., & Husbands, P. (2021). The role of rebound spikes in the maintenance of self-sustained neural spiking activity. *Nonlinear Dynamics*, *105*, 767–784. 10.1007/s11071-021-06581-2

Sarracino, A., Arviv, O., Shriki, O., & de Arcangelis, L. (2020). Predicting brain evoked response to external stimuli from temporal correlations of spontaneous activity. *Physical Review Research*, *2*(3), 033355. 10.1103/PhysRevResearch.2.033355

Shannon, C. E. (1948). A mathematical theory of communication. *Bell System Technical Journal*, *27*, 379–423, 623–656.

Sherrington, C. S. (1906). *The integrative action of the nervous system*. New Haven, CT: Yale University Press.

Shim, Y., & Husbands, P. (2015). Incremental embodied chaotic exploration of self-organized motor behaviors with proprioceptor adaptation. *Frontiers in Robotics and AI*, *2*, 7. 10.3389/frobt.2015.00007

Sporns, O. (2010). *Networks of the brain*. Cambridge, MA: MIT Press.

Strogatz, S. H. (2000). From Kuramoto to Crawford: Exploring the onset of synchronization in populations of coupled oscillators. *Physica D: Nonlinear Phenomena*, *143*(1–4), 1–20. 10.1016/S0167-2789(00)00094-4

Strogatz, S. H. (2001). Exploring complex networks. *Nature*, *410*(6825), 268. 10.1038/35065725, PubMed: 11258382

Tomov, P., Pena, R. F., Roque, A. C., & Zaks, M. A. (2016). Mechanisms of self-sustained oscillatory states in hierarchical modular networks with mixtures of electrophysiological cell types. *Frontiers in Computational Neuroscience*, *10*, 23. 10.3389/fncom.2016.00023, PubMed: 27047367

Vogels, T. P., Rajan, K., & Abbott, L. (2005). Neural network dynamics. *Annual Review of Neuroscience*, *28*(1), 357–376. 10.1146/annurev.neuro.28.061604.135637, PubMed: 16022600

Walter, W. G. (1950). The Twenty-Fourth Maudsley Lecture: The functions of electrical rhythms in the brain. *Journal of Mental Science*, *46*(402), 1–31. 10.1192/bjp.96.402.1

Wilson, H. R., & Cowan, J. D. (1973). A mathematical theory of the functional dynamics of cortical and thalamic nervous tissue. *Biological Cybernetics*, *13*(2), 55–80.

Zagha, E., Casale, A., Sachdev, R., McGinley, M., & McCormick, D. (2013). Motor cortex feedback influences sensory processing by modulating network state. *Neuron*, *79*(3), 567–578. 10.1016/j.neuron.2013.06.008, PubMed: 23850595

Received January 27, 2021; accepted September 21, 2021.